Human full-length coagulation factor X and a GLA domain-derived 40-mer polypeptide bind to different regions of the adenovirus serotype 5 hexon capsomer.

Sudir Sumarheni, Saw See Hong, Véronique Josserand, Jean-Luc Coll, Pierre Boulanger, Guy Schoehn, Pascal Fender

HUMAN GENE THERAPY 25:339–349 (April 2014)

DOI: 10.1089/hum.2013.222

Human Full-Length Coagulation Factor X and a GLA Domain-Derived 40-mer Polypeptide Bind to Different Regions of the Adenovirus Serotype 5 Hexon Capsomer

Sudir Sumarheni,[1,*] Saw See Hong,[2,3] Véronique Josserand,[4,5] Jean-Luc Coll,[4,5] Pierre Boulanger,[2] Guy Schoehn,[1,6] and Pascal Fender[1]

Abstract

The interaction of human adenovirus (HAdV)-C5 and many other adenoviruses with blood coagulation factors (e.g., human factor X, FX) involves the binding of their GLA domain to the hexon capsomers, resulting in high levels of hepatotropism and potential hepatotoxicity. In this study, we tested the possibility of preventing these undesirable effects by using a GLA-mimicking peptide as a competitor. An FX GLA domain-derived, 40-mer polypeptide carrying 12 carboxyglutamate residues was synthesized (GLA^{mim}). Surface plasmon resistance (SPR) analysis showed that GLA^{mim} reacted with free and capsid-embedded hexon with a nanomolar affinity. Unexpectedly, GLA^{mim} failed to compete with FX for hexon binding, and instead significantly increased the formation of FX–hexon or FX–adenovirion complexes. This observation was confirmed by *in vitro* cell transduction experiments using HAdV-C5-Luciferase vector (HAdV5-Luc), as preincubation of HAdV5-Luc with GLA^{mim} before FX addition resulted in a higher transgene expression compared with FX alone. HAdV-C5 virions complexed with GLA^{mim} were analyzed by cryoelectron microscopy. Image reconstruction demonstrated the *bona fide* hexon–GLA^{mim} interaction, as for the full-length FX, although with considerable differences in stoichiometry and relative location on the hexon capsomer. Three extra densities were found at the periphery of each hexon, whereas one single FX molecule occupied the central cavity of the hexon trimeric capsomer. A refined analysis indicated that each extra density is found at the expected location of one highly variable loop 1 of the hexon, involved in scavenger receptor recognition. HAdV5-Luc complexed with a bifunctional GLA^{mim}RGD peptide showed a lesser hepatotropism, compared with control HAdV5-Luc alone, and efficiently targeted $\alpha\beta$-integrin-overexpressing tumor cells in an *in vivo* mouse tumor model. Collectively, our findings open new perspectives in the design of adenoviral vectors for biotherapy.

Introduction

The human adenoviruses (HAdVs) are divided into species A to G, covering 51 different serotypes. The members of species C (e.g., HAdV-C2, HAdV-C5) and species B (HAdV-B3, HAdV-D35) are the most studied and characterized in terms of capsid structure, cell entry mechanisms, cellular response, and gene transfer [reviewed in (Russell, 2009)]. The capsid is composed of 11 well-identified structural proteins, of which the hexon is the major component: 240 copies of hexon form the 20 facets and 30 edges of the icosahedral capsid. The penton is the second most represented capsid protein, with 12 copies of penton located at each apex. Each penton capsomer is made up of a

[1]Centre National Recherche Scientifique, Université Joseph Fourier, European Molecular Biology Laboratory (Unit of Virus Host Cell Interactions; Unité Mixte Internationale-3265), 38042 Grenoble, France.
[2]Institut National Recherche Agronomique, Unité Mixte Recherche-754, Université Lyon 1, 69366 Lyon, France.
[3]Institut National de la Santé et de la Recherche Médicale, 75013 Paris, France.
[4]Institut Albert Bonniot, Institut National de la Santé et de la Recherche Médicale U823, 38706 Grenoble Cedex, France.
[5]Institut Albert Bonniot, Université Joseph Fourier, 38706 Grenoble Cedex, France.
[6]Centre National Recherche Scientifique, Université Joseph Fourier, Commissariat Energe Atomique (Institut Biologie Structurale; Unité Mixte Recherche 5075), 38027 Grenoble, France.
**Present address:* Faculty of Pharmacy, Hasanuddin University, Makassar 90245, Indonesia.

fiber, anchored to a pentameric protein, the penton base, closing up the vertices of the icosahedron. The cell entry pathway of HAdVs involved two steps. First, fiber interacts with an attachment receptor, for example, CAR, CD46, DSG-2, or proteoglycan, of which the specificity of recognition varies among the serotypes (Bergelson *et al.*, 1997; Sirena *et al.*, 2004; Marttila *et al.*, 2005; Nilsson *et al.*, 2011; Wang *et al.*, 2011). The secondary interaction of the penton base RGD motifs with cellular integrins, acting as internalization receptors, mediates the endocytosis of the virus (Belin and Boulanger, 1993; Wickham *et al.*, 1993; Gout *et al.*, 2010).

Adenoviruses are the most used vectors in human gene therapy trials. Since they are nonintegrative viruses, *ex vivo* strategies of re-engineering target cells are excluded, and most of the gene therapy protocols require *in situ* injection or systemic injection of therapeutic vectors in the bloodstream. This latter way of administration suffers from several drawbacks, in particular a high liver uptake of the vector, and consequently a poor availability for target cells or tissues. Alternative strategies have been proposed to overcome this hurdle, including the design of vector mutants or chimeras, but the results have been somewhat disappointing [reviewed in (Coughlan *et al.*, 2010)].

Recent breakthrough in the understanding of HAdV-C5–host interactions has shown that the vector particle accumulation in the liver is the result of HAdV-C5 binding to human blood coagulation factor X (FX) via the hexon capsomers, followed by the interaction of the HAdV-C5–FX complexes to heparan sulfate proteoglycan (HSPG) molecules that are present in a high concentration at the surface of the Kupffer cells (Vigant *et al.*, 2008; Waddington *et al.*, 2008; Alba *et al.*, 2010). To overcome this limitation, different strategies have been envisaged: (1) the use of HAdV serotypes (or HAdV-C5-based chimeric vectors), which are naturally (or artificially) nonbinders of blood coagulation factors (Waddington *et al.*, 2008); (2) mutations in the wild-type HAdV-C5 hexon to prevent FX binding (Bradshaw *et al.*, 2012; Doronin *et al.*, 2012); and (3) the design of molecules that compete with FX for hexon binding (Khare *et al.*, 2012; Duffy *et al.*, 2013). Although relatively less studied, the latter strategy has recently regained some interest, after the observation that FX can shield HAdV-C5 from the attack by the innate immune system (Xu *et al.*, 2013).

In this study, we investigated the effects of using a synthetic peptide (the GLA domain of human FX consisting of a 40-mer polypeptide biotinylated at its C-terminus [GLA^{mim}]) mimicking the FX-GLA domain as a competitor to FX during HAdV-C5-mediated cell transduction. We found that although GLA^{mim} was capable of binding to the hexon protein with a high affinity (in the nanomolar range), it was not able to compete with FX for hexon binding. Surface plasmon resistance (SPR) and cell transduction experiments suggested that FX and the GLA^{mim} peptide bound to separate sites on the hexon capsomer. Three-dimensional reconstruction of cryoelectron microscopy images of GLA^{mim}–adenovirion complexes taken at high resolution demonstrated that a GLA^{mim}-induced extra density is at the periphery of the hexon molecule, whereas full-length FX has been shown to bind to its central cavity. The extra density location coincided with highly variable loop 1 (HVR-1), a highly accessible and variable loop of the hexon capsomer, which was recently reported to be involved in scavenger receptor recognition (Khare *et al.*, 2012). Using an *in vivo* mouse tumor model, we found that the systemic administration of HAdV5-Luc in complex with a bifunctional GLA^{mim}RGD peptide resulted in a modest but significant liver detargeting, but efficient vector targeting to $\alpha\beta$-integrin-overexpressing tumor cells. Our results with the FX-derived GLA^{mim} peptide and a bivalent targeting peptide including GLA^{mim} open the path to new perspectives and new strategies in the design of rational adenoviral vectors for biotherapy.

Materials and Methods

Cells and virus

HeLa cells (European Cell Culture Collection) were cultured in Dulbecco's modified essential medium (DMEM) supplemented with 10% fetal calf serum, 2 m*M* L-glutamine (Glu), and 100 U/ml penicillin and 100 μg/ml streptomycin. HAdV5Luc, a replicative HAdV-C5 vector carrying the luciferase gene driven by CMV promoter inserted in the E3 region (Mittal *et al.*, 1993), was used in all experiments. For luciferase quantification, 48-well plates (Falcon) were seeded with 2×10^4 cells, 1 day before infection. Wells were infected at 100 vp/cell in 200 μl of medium without serum for 1 hr. Five hours postinfection, cell lysate was recovered in 100 μl cell lysis buffer (Promega) and luciferase activity was quantified using the Luciferase assay system (Promega) on a Victor^2 (Wallac) luminometer. Results were given as the mean of triplicates with standard deviation. For experiments with FX, virus samples were preincubated for 30 min at room temperature with either 8 or 0.08 μg/ml of human FX (Cryopep) directly or after a previous preincubation with 10 μg/ml of GLA^{mim} peptide.

GLA^{mim} peptide

The GLA^{mim} was synthesized by GENPEP and purified by high-performance liquid chromatography. GLA^{mim} contained 12 γ-carboxyglutamate residues at their exact positions in human FX. A biotin tag (GLA^{mim}), or the tripeptide sequence RGD (GLA^{mim}/RGD) was added at the C-terminus with a free NH_2 group. The GLA^{mim} sequence is depicted in Fig. 1A.

Isolation of HAdV-C5 virions and hexon capsomers

HAdV-C5 virions were recovered from HAdV-C5-infected HeLa cells, and purified by a conventional method including a double cycle of CsCl banding (Franqueville *et al.*, 2008). The native, trimeric hexon protein was recovered from the cell lysate and purified by a three-step procedure, as previously described (Boulanger and Puvion, 1973; Molinier-Frenkel *et al.*, 2000, 2002). Purification was checked by conventional sodium dodecyl sulfate polyacrylamide gel electrophoresis and Coomassie blue staining, and Western blot analysis using rabbit antibodies against antihexon or anti-HAdV-C5 whole virion, as previously described (Franqueville *et al.*, 2008; Corjon *et al.*, 2011).

Negative-staining and transmission electron microscopy

HAdV-C5 virions and hexon capsomers were quality controlled by negative-staining and transmission electron microscopy (TEM). The standard mica-carbon preparation

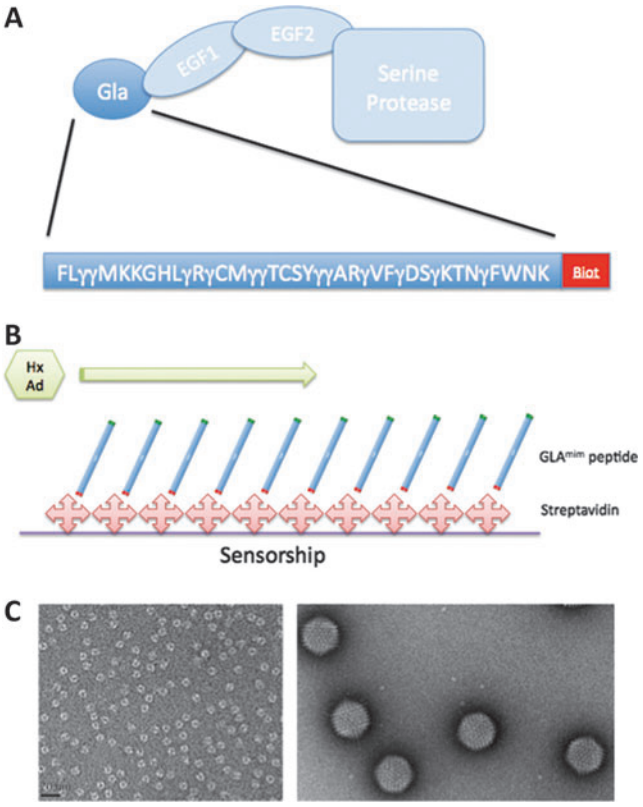

FIG. 1. Presentation of the partners. **(A)** Schematic of the different domains of the human factor X (FX). The biomimetic GLA^{mim} peptide reproduces the sequence of the FX GLA domain. It contains 12 gamma-carboxyglutamate residues (γ) and carries a biotinyl group at its C-terminal end. **(B)** Schematic representation of the GLA^{mim} peptides immobilized on streptavidin-coated Biacore sensor chip. The hexagonal box and the arrow depict the flow of ligands in solution or suspension, hexon protein (Hx) or HAdV-C5 virions (Ad), injected for SPR analysis. Note the upward orientation of the GLA^{mim} N-terminus. **(C)** Electron micrographs of purified HAdV-C5 hexon capsomers (left panel), and HAdV-C5 virions (right panel). Color images available online at www.liebertpub.com/hum

was used with the protein at 0.1 mg/ml or virion diluted 10 times after CsCl purification. Samples were stained by uranyl acetate and observed under a Phillips CM12 electron microscope at 120 kV.

SPR experiments

All SPR experiments were performed in a running buffer composed of HBS buffer (GE Healthcare) supplemented by 2 m*M* $CaCl_2$ (HBS-Ca) at a flow rate of 5 μl/min on a BIAcore 3000 instrument (GE Healthcare). Surface immobilization was done by the standard EDC-NHS activation (GE Healthcare) for 10 min followed by injection of the ligand either streptavidin or human FX at 1 μg/ml in 10 m*M* acetate buffer pH 4.5 for 10 min (4,100 and 4,200 RU, respectively). Blocking was done by a 10 min inactivation with 1 *M* ethanolamine. For GLA experiments, biotinylated GLA^{mim} peptide was injected at 10 μg/ml for 10 min in HBS-Ca (1,080 RU). When FX was used as the ligand (4,200 RU), the negative controls for background subtraction consisted of EDC-NHS inactivated flow cell. When GLA^{mim} peptide was used as the ligand, negative controls used streptavidin-coated flowcell. In all experiments (done in triplicate), surface regeneration was done by a two-time injection of 10 m*M* HCl for 2 min. Between two injections, there was a stabilization period in HBS-Ca for 15 min.

Cryo-EM

HAdV-C5 virions were incubated in 10 m*M* Hepes buffer pH 7.4 supplemented with 2 m*M* $CaCl_2$ and a 10-fold molar excess of GLA^{mim} peptide. After 1 hr incubation, the excess peptide was eliminated by dialysis. Four microliters of the sample (either HAdV-C5 or HAdV-C5–GLA^{mim}) was loaded onto a Quantifoil R2/1 holey grid (Quantifoil Micro Tools GmbH), vitrified using a Mark IV vitrobot (FEI). The frozen grid was transferred into a Polara electron microscope working at 300 kV. The images were taken under low-dose conditions (<20 $e^-/Å^2$) and with a nominal magnification of 31,000 on KODAK SO-163 films. The negatives were developed in full-strength D19 developer for 12 min.

Image analysis

Negatives were screened for astigmatism and drift by optical diffraction, and only those (33 negatives in total for HAdV-C5–GLA^{mim}, 30 for HAdV-C5 alone) showing information up to 7 Å were digitized using a Photoscan TD scanner with a pixel size of 7 mm (2.25 Å per pixel at the specimen level). The particles were selected interactively using x3d (Conway and Steven, 1999) boxed into 447×447 pixel squares and corrected for the contrast transfer function effect as previously described (CTFMIX) (Fabry *et al.*, 2005). Particle origin and orientation were determined with the model-based PFT2 programs using a previously determined and scaled to the right size 3D structure of HAdV-C5 as a starting model (Fabry *et al.*, 2005). The final reconstructions were calculated using EM3DR2 (Fuller *et al.*, 1996) with a total of 4,762 particles (about 66% of the total) for HAdV-C5–GLA^{mim} and 3,648 particles (about 66% of the total) for HAdV-C5. The resolution of the final maps was estimated to be about 9 Å by Fourier shell correlation (not shown).

Animal tumor model

All animal experiments were conducted in agreement with the *Principles of Laboratory Animal Care* (NIH Publication No. 86-23, revised 1985). HEKb3 is a cell line derived from the original HEK-293 cell line (human embryonic kidney cells) stably expressing the β3 integrin subunit. HEKβ3 cells were cultured at 37°C in a humidified 95% air–5% CO2 atmosphere in DMEM supplemented with 10% fetal bovine serum. HEKβ3 were harvested, washed, and resuspended in phosphate buffered saline at 10^7 cells/200 μl for subcutaneous implantation in the right posterior limb of anesthetized (isoflurane) NMRI nude mice (female, 6 weeks old).

In vivo *bioluminescence imaging*

Subcutaneous HEKβ3 tumor growth was followed by caliper measurements once a week. When tumor size reached about 500 mm^3 (about 8 weeks), the mice were randomized and divided into three groups. Aliquots of HAd5-Luc vector (4×10^{10} vp/mouse) alone or in combination with GLA^{mim} or

$GLA^{mim}RGD$ peptide (10 μg/ml in 10 m*M* Hepes buffer pH 7.4–2 m*M* $CaCl_2$) were injected (100 μl) in the tail vein after a 30 min incubation at room temperature. The theoretical number of peptide binding sites is about 3×10^{13} for 4×10^{10} vp. Considering that the GLA^{mim} or $GLA^{mim}RGD$ peptides have a molecular mass around 6 kDa, the dose of 1 μg per injection corresponded to 1×10^{14} molecules, equivalent to a threefold excess over the theoretical binding sites on the vector.

Luciferase expression was monitored by *in vivo* bioluminescence 24, 48, and 72 hr after the intravenous injection. Vigil mice were injected intraperitoneally with 150 mg/kg of D-Luciferin (Promega) just before anesthesia (isoflurane 4% for induction and 1.5% thereafter). Five minutes after luciferin administration, bioluminescence images were acquired with an IVIS KINETIC (Perkin Elmer). Quantitative analysis was carried out using Living image software (Perkin Elmer). The results were expressed as the number of photons per second (ph/sec).

Results

GLA^{mim} peptides, HAdV-C5 virions, and hexon capsomers

The sequence of the polypeptide selected to mimic GLA^{mim} corresponding to amino acid residues 4–43 of the human FX amino acid sequence (Fig. 1A). The rationale for the design of a GLA^{mim} polypeptide lacking the N-terminal tripeptide A-N-S was to use a minimal GLA domain including the 12 conserved γ-carboxyglutamate residues common to 2 hexon binders, the human FIX and FX. The N-terminal A-N-S tripeptide is not conserved in FIX and FX, and is replaced by Y-N-S-G in FIX. By contrast, the 12 γ-carboxyglutamate residues are strictly conserved in human FX and FIX, and conserved to more than 75% in other human GLA domain-containing proteins, such as FVII, prothrombin, protein C, and protein S (Sunnerhagen *et al.*, 1995).

Two different polypeptides were synthesized: (1) The princeps molecule described above (biotinylated GLA^{mim}) used in SPR studies, so that the GLA^{mim} molecules will react with surface-coated streptavidin with the desired orientation for maximum accessibility (Fig. 1B). (2) For cell targeting assays with a dual-specificity peptide (viral and cellular), the tripeptide RGD was added to the C-terminus in lieu of the biotin radical, as the ligand of cellular integrins ($GLA^{mim}RGD$). HAdV-C5 virions and hexon capsomers used for the SPR analysis with the GLA^{mim} peptide were both tested for their integrity and purity by negative staining and electron microscopy (Fig. 1C).

SPR analysis of GLA^{mim}–hexon interaction

The interaction of the GLA^{mim} peptide to hexon proteins was first validated by SPR analysis. The biotin-tagged GLA^{mim} peptide of 6 kDa was immobilized on a streptavidin-coated CM4 sensor chip, with its N-terminus oriented upward, as depicted in Fig. 1B. The control flowcells used for background subtraction were coated with streptavidin alone. The hexon protein was injected at different concentrations ranging from 30 to 120 n*M* in the presence of $CaCl_2$ (Fig. 2A). The dose–response sensorgrams obtained showed a rapid association rate ($k_a = 1.9\times10^5$ *M*/sec) and a slow dissociation rate ($k_d = 3.3\times10^{-3}$/sec). Fitting of these sensorgrams using BIAeval software gave an equilibrium constant

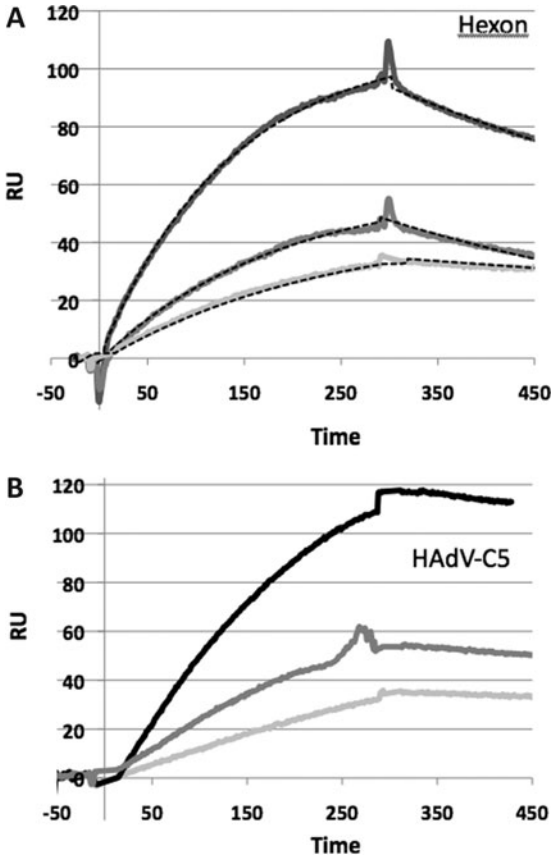

FIG. 2. SPR analysis of the binding of hexon capsomers and HAdV-C5 virions to surface-immobilized GLA^{mim}. **(A)** Hexon dose-dependent response at 30, 60, and 120 n*M*, respectively. Fits of data using BIAeval software are shown as superimposed dotted lines (1:1 Langmuir binding analysis gave the following values: $K_{ass} = 1.9\times10^5/M\cdot$sec; $K_{diss} = 3.3\times10^{-3}$/sec; $K_D = 17.3$ n*M*). **(B)** Virion dose-dependent response at 5×10^9, 1×10^{10}, and 2×10^{10} vp/ml, respectively. vp, virus particles.

of $K_D = 17$ n*M* for the binding reaction of hexon capsomer to the GLA^{mim} peptide (Fig. 2A). A highly efficient regeneration of the sensor chip, with complete release of hexon capsomers from the flowcell, was achieved using 10 m*M* EDTA for 2 min (Supplementary Fig. S1; Supplementary Data are available online at www.liebertpub.com/hum). This suggested that the hexon–GLA^{mim} binding involved electrostatic interactions and required calcium chelation by both partners. Interestingly, a ''reverse binding experiment'' in which the hexon was immobilized on the sensor chip also showed that FX binding was enhanced by the GLA^{mim} peptide (Supplementary Fig. S2). This experiment confirmed that the GLA^{mim} peptide effectively enhanced the FX–hexon binding and that this effect was not caused by the analyte aggregation on the sensor chip surface. Moreover, this effect occurred rapidly since in the ''reverse binding experiment,'' GLA^{mim} and FX were coinjected on immobilized hexon at the same time.

The interaction of HAdV-C5 virions with immobilized GLA^{mim} was also investigated by injection of different concentrations of HAdV-C5 virions, ranging from 1 to 4×10^{10} vp/ml. HAdV-C5 binding was detected for all the

concentrations tested, and the intensities of the signals correlated with the different virus concentrations (Fig. 2B). Again, the return to the baseline occurred upon EDTA regeneration, but required a longer injection time (5 min) compared with free hexon capsomers. This was consistent with an avidity effect that could take place between the 12 hexon trimers forming the adenoviral facets and the GLA^{mim} peptide-coated surface of the sensor chip. This avidity effect was evident on sensorgrams recorded at the end of injections: the absence of dissociation observed for the whole virus suggested a very strong interaction between the virion and the immobilized GLA^{mim}, likely because of multivalent interactions between the hexon facets and the sensor chip surface. The SPR analysis therefore validated the functionality of the GLA^{mim} peptide in terms of specific interaction with the HAdV-C5 capsid, via a high-affinity binding to the hexon capsomers.

Competition between GLA^{mim} and FX for hexon binding: SPR analysis

Hexon protein. We next explored the capacity of the GLA^{mim} peptide to compete with FX for binding to the isolated or capsid-incorporated hexon protein, using an SPR setup in which human FX was immobilized onto the sensor chip. As control, a solution of the hexon protein at different concentrations (ranging from 0.8 to 66 n*M*) was injected. As expected from our previous study (Corjon *et al.*, 2011), the sensorgram showed an efficient binding of hexon to FX (Fig. 3A). Surprisingly, when the hexon solution at the same concentrations was preincubated with GLA^{mim} at 10 μg/ml

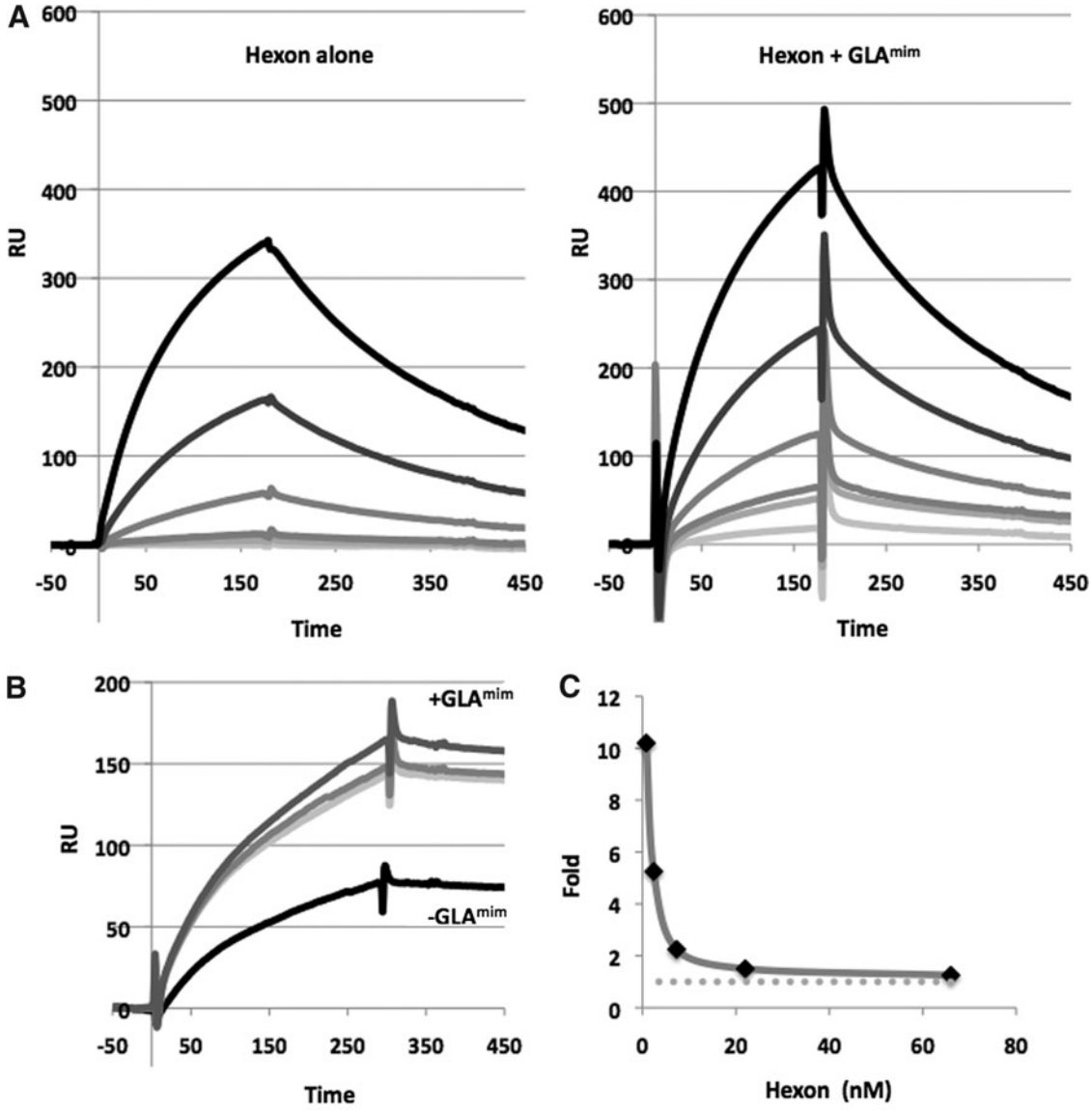

FIG. 3. SPR analysis of the binding of hexon capsomers to immobilized FX, in the presence or absence of GLA^{mim}. **(A)** Sensorgrams after injection of hexon alone, ranging from 0.9 to 66 n*M*, or after preincubation with 1.6 μM GLA^{mim}. **(B)** A fixed concentration of hexon (16 n*M*) was injected alone (control without GLA^{mim}, black curve) or after 30 min preincubation with 1600, 160, or 16 n*M* of GLA^{mim} peptide. **(C)** Plot of the values of ratios of RU_{max} (with GLA^{mim} vs. without GLA^{mim}) at the different concentrations of hexon tested.

(1.6 μM) before injection, a significant increase in the intensity of the SPR signal was observed (Fig. 3A). The higher signal observed in the presence of GLA^{mim} was not an effect caused by the peptide mass. Whatever the stoichiometry of hexon-bound GLA^{mim} to hexon, that is, 1 GLA^{mim} molecule (6 kDa) to 1 hexon trimer (330 kDa) or 1 GLA^{mim} to 1 hexon monomer (110 kDa), the ratio of peptide-to-hexon protein would only represent 5.5–1.8% of the total mass. Moreover, GLA^{mim} was not the limiting factor in this experiment, and when lower concentrations of GLA^{mim} (down to 16 nM) were used, the enhancing effect on the binding of hexon to FX was still observed (Fig. 3B).

Interestingly, the enhancing effect of GLA^{mim} on hexon binding was higher at lower hexon concentrations ($\geq$10-fold), and progressively decreased in a hexon dose-dependent manner (Fig. 3B and C). In the sensorgrams, an SPR signal of hexon binding to FX was detectable for hexon concentrations below 2.4 nM in the presence of GLA^{mim}, whereas no signal was observed for the same hexon concentrations in the absence of GLA^{mim} (Fig. 3A). Collectively, our data suggested that the affinity of hexon toward FX was higher in the presence of GLA^{mim} compared with its binding affinity in the absence of GLA^{mim}: a value of about 2 nM has been reported in previous studies (Vigant *et al.*, 2008; Waddington *et al.*, 2008).

HAdV-C5 virions. Similar SPR analysis was then performed using HAdV-C5 virions and immobilized FX. Preincubation of GLA^{mim} with virions significantly enhanced their binding to FX, $\sim$3-fold for the low virus input (Fig. 4A, left panel), compared with 1.2-fold for the higher virus input (Fig. 4A, right panel). Again, this effect cannot be explained by an effect of the peptide mass, which was negligible compared with the whole virus particle. These results confirmed those obtained with isolated hexon capsomers.

Competition between GLA^{mim} and FX for hexon binding: cellular assays

Our next experiment was designed to determine whether GLA^{mim} could have an effect, positively or negatively, on HAdV-C5-mediated cell transduction in the presence of FX at physiological concentrations. HeLa cells were incubated at 37°C for 1 hr with constant inputs of HAdV5-Luc vector, complexed or not with their ligands. HAdV5-Luc was preincubated with FX at physiological (8 μg/ml) or subphysiological (0.08 μg/ml) concentrations, alone or with variable GLA^{mim} concentrations. Cell transduction efficiency was then evaluated from the level of luciferase activity at 5 hr postinfection. At this early time, the genome replication had not started, and only the efficacy of the cellular uptake of the vector was measured.

As expected, incubation of HAdV5-Luc with FX at the physiological concentration resulted in a sixfold increase in the luciferase expression (Fig. 4B, right panel). However, preincubation of HAdV5-Luc with GLA^{mim} before FX at the physiological concentration resulted in an extra twofold increase in the luciferase signal (Fig. 4B, right panel). This was consistent with the SPR data showing an enhancing effect of GLA^{mim} on the FX–hexon interaction. FX used at the subphysiological concentration showed no detectable effect on HAdV5-Luc-mediated cell transduction (Fig. 4B, left panel). Importantly, a significant enhancing effect on luciferase expression was detected upon GLA^{mim} addition (1.5-fold; Fig. 4B, left panel). This result confirmed the SPR data (refer to Figs. 3C and 4B), and indicated that the presence of GLA^{mim} peptide made detectable the hexon–FX interaction, which would otherwise remain undetectable with FX alone.

Cryo-EM analysis

We next examined HAdV-C5-GLA^{mim} complexes by cryo-EM, in comparison with HAdV-C5 alone (Fig. 5). The rationale for this analysis was that the identification of the binding sites of GLA^{mim} on the viral capsid might help to elucidate the molecular mechanism of the effect of this peptide on hexon– and adenovirion–FX interaction. Strong extra densities, absent from control HAdV-C5, were clearly visible on the hexon capsomers of the HAdV-C5-GLA^{mim} complexes (Fig. 5B and C). Interestingly, three extra densities were found per hexon capsomer (Fig. 5D). More importantly, these extra densities were located at the periphery of the hexon capsomer and not in the cavity of hexon, where FX had been previously localized (Waddington *et al.*, 2008; Irons *et al.*, 2013) (Fig. 5B and D). The HAdV-C5 capsid 3D map has been deposited in the Macromolecular Structure Database (Accession No. EMD-2568).

When compared with the X-ray structure of hexon crystals, the extra densities were found to be located in the invisible regions assigned to the HVR1 loops (Fig. 5E). Although the HVR1 loop structure has been solved neither by X-ray crystallography nor by cryoEM image analysis, our three-dimensional reconstruction strongly suggested that the extra densities visible on the hexon capsomers were because of GLA^{mim} peptides, either directly or indirectly. In the latter case, the GLA^{mim} peptide would induce some rigidity and/or reorganization of the secondary structure of the intrinsically disordered HVR1 loop.

Hepatotropism and tumor targeting in vivo *in a mouse model*

As the GLA^{mim} peptide interacted with HAdV-C5 at 720 copies/virion, we next investigated if a bivalent peptide comprising of two entities, the viral ligand GLA^{mim} on the N-terminal side, coupled to a cell surface ligand on the C-terminal side, could be used to redirect the HAdV5-Luc vector to a specific cell target. To this aim, a tripeptide RGD was added to the exposed C-terminus of the GLA^{mim} peptide (GLA^{mim}RGD), and the HAdV5-Luc–GLA^{mim}RGD complex was tested *in vivo* in a mouse tumor model, in which mice were engrafted with HEKβ3 cells overexpressing human $\alpha\beta$-integrins. When the tumor size reached about 500 mm^3, the mice were intravenously injected with HAdV5-Luc alone or with HAdV5-Luc preincubated with GLA^{mim} or GLA^{mim}RGD. The level of luciferase expression was monitored by noninvasive whole-body imaging over 3 days, and quantitatively determined in the liver and grafted tumor (Supplementary Fig. S3 and Fig. 6A).

With control HAdV5-Luc alone, the bioluminescent signal was localized massively within the liver (Supplementary Fig. S3A). With the HAdV5-Luc–GLA^{mim} complex, we observed a 2–3-fold lower luminescent signal in the liver, compared with the HAdV5-Luc vector alone. This effect was detected

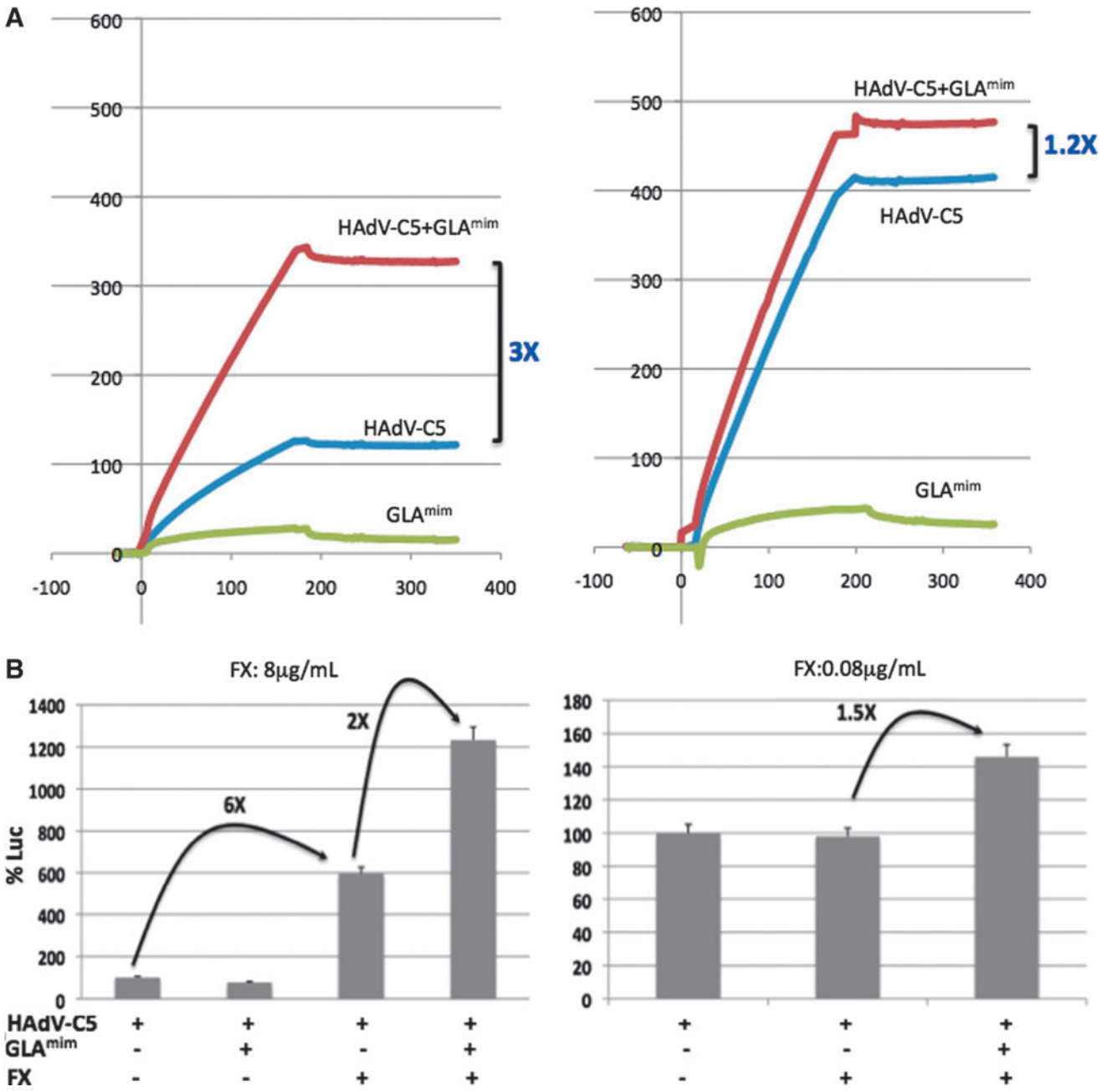

FIG. 4. Influence of GLA^{mim} on the binding of HAdV-C5 virions to immobilized FX and influence on the HAdV5-Luc vector-mediated transduction. **(A)** FX- HAdV-C5 binding. Sensorgrams of HAdV-C5 injection at 2×10^9 vp/ml (left panel) and 1×10^{10} vp/ml (right panel) to immobilized FX. The different sensorgrams shown in different colors represent the signals obtained with the virus alone (blue), virus preincubated with 1.6 μM GLA^{mim} (red), and GLA^{mim} alone at 1.6 μM (green). **(B)** Luciferase expression: The luciferase activity was assayed in lysates of HeLa cells infected with HAdV5-Luc vector and harvested at 5 hr postinfection. HAdV5-Luc was used alone, or after preincubation for 30 min with FX alone or FX + GLA^{mim} (1.6 μM), as indicated in the *x*-axis. Left panel: The physiological concentration of FX (8 μg/ml; 160 nM); right panel: Similar experiments were performed at the subphysiological concentration of FX (0.08 μg/ml; 1.6 nM). The value of 100% luciferase expression was given by cell samples transduced by HAdV5-Luc alone. Results are given as mean + SD from triplicate experiments. Color images available online at www.liebertpub.com/hum

at 24 and 48 hr postinjection, and persisted until day 3. A reduced hepatotropism, compared with the control, was also observed with the HAdV5-Luc–GLA^{mim}RGD complex, but mainly at late times after injection (Supplementary Fig. S3A).

In parallel to its decrease in the liver, the luciferase activity increased significantly over time in the HEKβ3 tumors of mice injected with HAdV5-Luc–GLA^{mim}RGD ($\sim$2-fold), compared with control groups injected with HAdV5-Luc alone or HAdV5-Luc–GLA^{mim} complex (Supplementary Fig. S3B). At each time point, the tumor-to-liver signal ratio was significantly higher in mice administered with HAdV5-Luc complexed with GLA^{mim}RGD, compared

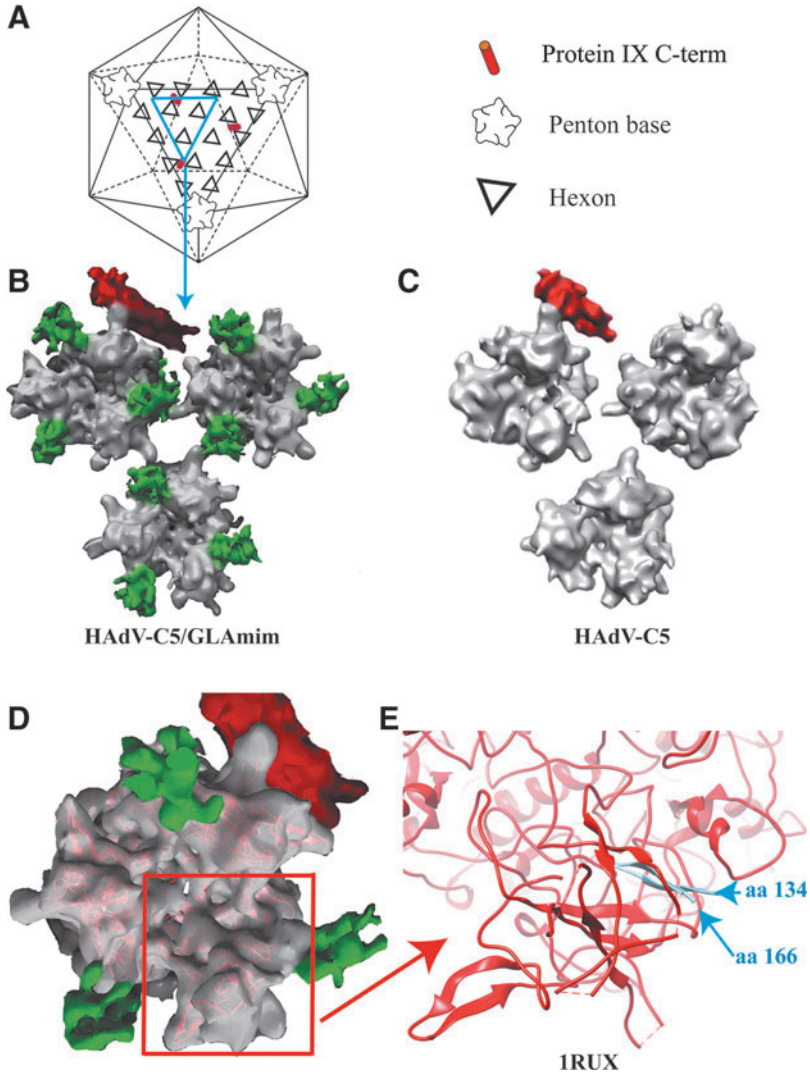

FIG. 5. Three-dimensional (3D) reconstruction of HAdV-C5–GLA^{mim} complexes from Cryo-EM images. **(A)** Schematic organization of adenovirus capsomers within the adenoviral icosahedron. **(B)** Zoom on the region corresponding to the blue triangle highlighted in **(A)** for the HAdV-C5–GLA^{mim} 3D reconstruction. The three hexons are represented in gray, the C-terminal parts of protein IX are colored in red, and HVR1 loop–GLA^{mim} extra densities are highlighted in green. **(C)** Zoom on the region corresponding to the blue triangle highlighted in **(A)** for the HAdV-C5 3D reconstruction. **(D)** Fitting of the HAdV-C5 hexon atomic structure (PDB No. 1RUX) into the cryo-EM envelope. This panel shows that compared with the HAdV-C5 structure or the hexon X-ray structure, an extra density is visible. These extra densities corresponded to the putative location of the disordered HVR1 loop invisible in the hexon crystals. **(E)** Zoom on the region corresponding to the red rectangle in **(D)** for the atomic resolution structure of the hexon (PDB No. 1RUX). Amino acids 131–134 and 166–170 corresponding, respectively, to the start and to the end of the HVR1 loop, respectively, are highlighted in blue. Color images available online at www.liebertpub.com/hum

with HAdV5-Luc alone or HAdV5-Luc–GLA^{mim} complex (2–4-fold; Fig. 6B). This implied an increased retargeting of HAdV5-Luc to HEKβ3 cells, and a higher susceptibility of $\alpha\beta$-expressing tumor cells to HAdV5-Luc in the presence of GLA^{mim}RGD.

The results of our *in vivo* experiments were in apparent contradiction with our biochemical and *in vitro* cellular studies, showing an enhancing effect of GLA^{mim} on the FX–hexon binding and on HAdV5-Luc-mediated cell transduction in the presence of FX. However, recent data suggested the implication of HVR1 in the recognition of scavenger receptors by HAdV-C5 (Khare *et al.*, 2012), suggesting that GLA^{mim} could interfere with scavenger receptors for binding to hexon HVR1. However, to get a full view on the mechanism taking place after HAdV-C5–peptide injections, an immunocompetent model of mice would be required to investigate whether the GLA^{mim} peptide can shield the HAdV-C5 vector and thus prevent the sequential events of (1) nonneutralizing antibody binding, (2) complement activation, and (3) triggering of the innate response, as previously reported (Baker *et al.*, 2013; Xu *et al.*, 2013).

Discussion

After the discovery of the binding of blood coagulation factors to adenoviral vectors during systemic administration, and the resulting sequestration of the vectors within the liver, it appeared necessary to reconsider the conclusions of past clinical trials, and to develop new strategies to overcome this limitation for future biotherapy protocols. Blood coagulation factors bridge the hexon capsomers to ubiquitous cellular receptors, such as HSPGs present in high concentration at the surface of Kuppfer cells. Among the diverse strategies proposed to palliate this inconvenience, the development of molecules blocking this interaction has been less investigated (Chen *et al.*, 2010; Duffy *et al.*, 2013), compared with direct modifications of the coagulation factor binding site on the hexon capsomers (Vigant *et al.*, 2008; Waddington *et al.*, 2008). The present study is in line with the first type of experimental approach.

Intuitively, a peptide mimicking the region of interaction of FX with hexon, that is, the GLA domain, would be the ideal antagonist molecule of FX, as it would compete for the binding site on the hexon capsomer. To this aim, we

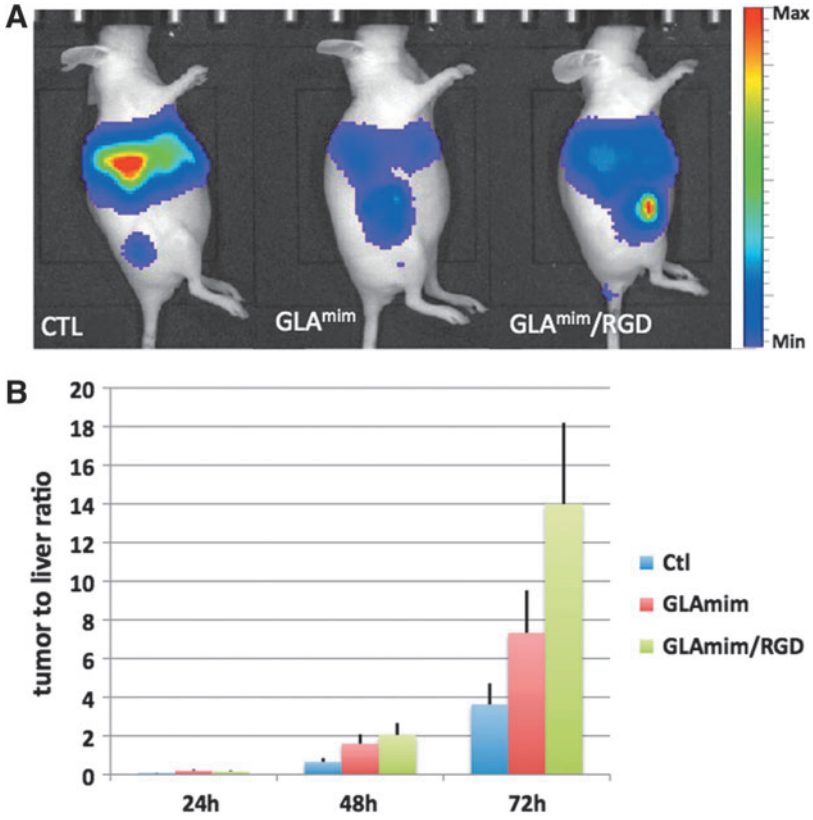

FIG. 6. Influence of GLA^{mim} peptides on the tissue tropism of a HAdV-C5-based vector in a mouse tumor model. Three groups of mice were engrafted in the right posterior limb with HEK-β cells. Each mouse received an aliquot (4×10^{10} vp) of HAdV5Luc vector (alone or complexed with GLA^{mim} or GLA^{mim}RGD peptides) by injection in the tail vein. **(A)** Noninvasive whole-body Imaging. The biodistribution of HAdV5-Luc vector was determined at different times after intravenous injection. The animals shown are representative of each group ($n=5$ mice per group) at 48 hr postinjection. **(B)** Vector distribution between tumor and liver. The mean bioluminescent signals were quantitated in the liver and the tumor at 24, 48, and 72 hr after the systemic administration of HAd5-Luc alone (control), or HAd5-Luc preincubated with GLA^{mim} or GLA^{mim}RGD peptide. The values of the tumor-to-liver signal ratios are plotted versus time postinjection. Shown in the histogram are mean (m) $\pm$ SEM ($n=5$). Color images available online at www.liebertpub.com/hum

designed a synthetic 40-mer polypeptide, GLA^{mim}, which mimicked the FX GLA domain including the carboxyglutamate residues at highly conserved positions in all GLA-domain-containing proteins, but lacking the first A, N, and S residues. The GLA^{mim} was tagged with a biotinyl group at its C-terminus, to promote its orientation on BIAcore sensor chips in an adenovirus accessible manner, that is, with its N-terminus exposed (refer to Fig. 1C). Chemical synthesis of GLA^{mim}, a 40-mer peptide carrying 12 carboxyglutamate residues, was a challenge, but the result obtained was a soluble, homogenous peptide that was found to be fully functional in terms of interaction with soluble hexons, or HAdV-C5 virions, based on conventional criteria and assays, such as SPR.

We found that hexon capsomers interacted with immobilized GLA^{mim} in a dose-dependent manner, with a dissociation constant in the nanomolar range ($K_D\approx17$ nM). Of note, in the original report (Waddington *et al.*, 2008), FX was found to bind to hexon with a K_D of ~2 nM. The eightfold lower affinity of GLA^{mim} for hexon, compared with that of full-length FX, was explained by the higher association rate of FX (2.3×10^6 M/sec vs. 1.9×10^5 M/sec for GLA^{mim}), while the dissociation rates were comparable for FX and GLA^{mim} (4.5×10^{-3}/sec and 3.3×10^{-3}/sec, respectively). HAdV-C5 virions also showed a strong interaction with the GLA^{mim}-coated surface, and the SPR plateau of persistent binding at the end of the HAdV-C5 injection suggested an avidity effect. This avidity effect was not surprising, considering the complexity and the multivalent nature of the viral ligand, which is made of 240 copies of trimeric hexons distributed between 20 capsid facets.

However, no blockage of FX–hexon interaction was observed with a large excess of GLA^{mim} in competition assays *in vitro* and *in cellulo*. Instead, GLA^{mim} increased the affinity of hexon for FX, as shown by SPR, and augmented the transduction efficiency of HeLa cells with HAdV5-Luc vector in the presence or absence of FX. These paradoxical results incited us to seek for structural information on the binding of GLA^{mim} to the adenoviral capsid, using cryo-EM. Density map comparison between control HAdV-C5 virions and HAdV-C5–GLA^{mim} complexes showed the presence of three extra densities per trimeric hexon capsomer. Our 3D reconstruction and the stoichiometry of 3:1 differed from the original model of HAdV-C5 virions in complex with full-length FX, which assigned only one FX molecule per trimeric hexon capsomer with a stoichiometry of 1:1 (Waddington *et al.*, 2008).

The greatest discrepancy between our reconstructed HAdV-C5–GLA^{mim} complex and the original FX-HAdV-C5 model resided in the topography of hexon-bound GLA^{mim} molecules, compared with hexon-bound FX. The FX molecule has been shown to occupy the central cavity of the hexon capsomer (Waddington *et al.*, 2008), and the FX binding involved side chains of amino acids located in the HVR7 loop, including T423, E424, and T425 (Doronin *et al.*, 2012; Irons *et al.*, 2013). In our 3D reconstruction of the HAdV-C5–GLA^{mim} complex, however, the three additional densities surrounded the central cavity and were localized to the undetermined regions in the hexon crystals that were assigned to HVR1 loops (residues 135–165). The extra densities could result from a direct or indirect effect of the GLA^{mim} peptide on HVR1. In the first case, the extra densities would correspond to the GLA^{mim} peptides themselves; in the other case, GLA^{mim} would induce some rigidity and/or secondary structure reorganization of the

intrinsically disordered HVR1 loops. Interestingly, the HVR1 loop is the most negatively charged in serotype 5 hexon, with a net charge of −13 amino acids. Upon GLA^{mim} binding, a rigidification/folding of HVR1 loop might offer a better access to the FX protein. This interaction likely required calcium chelation by both GLA^{mim} and HVR1 residues as suggested by the high efficiency of EDTA regeneration in the hexon–GLA^{mim} interaction studied by SPR experiments (Supplementary Fig. S1).

The A-N-S sequence, missing from GLA^{mim}, is highly conserved in FX throughout the vertebrate evolution, and play an important role in coordinating Ca^{2+} ions, and in stabilizing the N-terminal fold. However, it is unlikely that the lack of these three amino acids is responsible for the differential hexon binding activity between FX and GLA^{mim} for the following reasons: (1) human FIX also binds to hexon, but lacks the N-terminal peptide A-N-S (replaced by Y-N-S-G); (2) likewise, human FVII, another hexon binder (Irons *et al.*, 2013), starts with the A-N-A tripeptide sequence; (3) it has been recently shown that the critical residue for hexon binding is Lys10 (Doronin *et al.*, 2012), whereas the N-terminal hydrophobic cluster is involved in membrane binding (Sunnerhagen *et al.*, 1995).

Our data implied that two types of GLA-binding sites coexist on the same hexon capsomer, displayed by HVR7 and HVR1, respectively. The differential binding of full-length FX molecule versus GLA^{mim} to hexon capsomer remained to be elucidated. One clue might be given by the recent observation that the GLA domains of FX and FVII bind to different sites in the hexon cavity, enabling or not the dimerization of coagulation factors bound to adjacent hexons of the facet edges (Irons *et al.*, 2013). In the same line of hypotheses, the accessibility and/or reactivity of certain amino acid side chains might differ between full-length FX and its isolated GLA domain. Differences in the molecular mass of hexon ligands might also be evoked. Full-length FX molecule with its bulky serine-protease domain of 58 kDa would impair, by steric hindrance, the binding of more than one single FX molecule per hexon, resulting in only 240 copies of FX per virion. In contrast, GLA^{mim}, a small peptide of 6 kDa, could occupy all the available binding sites at the virion surface. In this case, however, the determinants of choice of the HVR1 sites by GLA^{mim}, instead of HVR7 or both HVR1 and HVR7, are unknown and require further studies.

Although our data invalidated our working hypothesis of using GLA^{mim} as an FX antagonist, the development of new therapeutic strategies might be envisaged, based on the specific properties of GLA^{mim}. One major feature and advantage of GLA^{mim} resided in its capacity to bind to the hexon capsomers of HAdV-C5 with high affinity and in high numbers (720 copies of GLA^{mim} per virion), to constitute a mantle of retargeting peptides around the viral capsid. When complexed with HAdV5-Luc, GLA^{mim} appeared to reduce its hepatotropism after systemic administration to mice, suggesting an interfering effect of GLA^{mim} with scavenger receptors for hexon binding via HVR1 (Khare *et al.*, 2012). This decrease implied that FX, HSPGs, and hexon HVR7 were not the only factors controlling the HAdV-C5 hepatotropism, and confirmed the results of a recent study (Khare *et al.*, 2012).

The results of our *in vivo* experiments were in apparent contradiction with our biochemical and *in vitro* cellular studies, showing an enhancing effect of GLA^{mim} on the FX-hexon binding and on HAdV5-Luc-mediated cell transduction in the presence of FX. However, recent data suggested the implication of HVR1 in the recognition of scavenger receptors by HAdV-C5 (Khare *et al.*, 2012), suggesting that GLA^{mim} could interfere with scavenger receptors for binding to hexon HVR1.

A similar level of liver detargeting was observed with GLA^{mim}RGD, a bivalent GLA^{mim}-containing peptide terminated by an RGD sequence. More interestingly, GLA^{mim}RGD retargeted the HAdV5-Luc vector to $\alpha v\beta 3$-integrin-overexpressing cells in a mouse tumor model *in vivo*. Thus, in combination with HAdV-C5 vectors mutated in the FX-binding site of HVR7, GLA^{mim}-containing bifunctional peptides might confer two advantages to the mutant vectors, the decrease of adverse effects because of the liver sequestration, and the gain of a new function, that is, a specific cell retargeting. In addition, as ligands of HVR1, GLA^{mim}-derived peptides would also represent valuable biological tools for investigating scavenger receptors exposed at the cell surface.

Our animal experiments were performed using tumor-bearing nude mice. A full view on the mechanism taking place after HAdV-C5–GLA-peptide injection would require an immunocompetent animal model, allowing to investigate whether the GLA^{mim} peptide can shield the HAdV-C5 vector, and thus prevent the sequential events of (1) of nonneutralizing antibody binding, (2) complement activation, and (3) triggering of the innate response, as observed with FX (Baker *et al.*, 2013; Xu *et al.*, 2013).

Acknowledgments

S.S. was supported by the ''Bio-Health Computing'' European training program. This work used the platforms of the Grenoble Instruct center (ISBG; UMS 3518 Centre National Recherche Scientifique (CNRS)-Commissariat Energie Atomique (CEA)-Université Joseph Fourier (UJF)-European Molecular Biology Laboratory (EMBL)) with support from FRISBI (ANR-10-INSB-05-02) and GRAL (ANR-10-LABX-49-01) within the Grenoble Partnership for Structural Biology. The electron microscope facility (Polara electron microscope) was supported by the Rhône-Alpes Region, the FRM, the CNRS, the University of Grenoble, and the GIS-IBISA.

The work at the UCBL-Institut National Recherche Agronomique Unité Mixte Internationale-754 was funded in part by the French Foundation for Cystic Fibrosis (Vaincre la Mucoviscidose; Contract VLM-RF2013-0500796). S.S.H. is a scientist of the French Institute of Health and Medical Research (Institut National de la Santé et de la Recherche Médicale, INSERM), and the recipient of a Contrat d'Interface INSERM-Hospices Civils de Lyon (CIF-2008–2013). We are most grateful to Jullien Vollaire and Mélanie Guidetti for their help with animal studies.

Author Disclosure Statement

No competing financial interests exist.

References

Alba, R., Bradshaw, A.C., Coughlan, L., *et al.* (2010). Biodistribution and retargeting of FX-binding ablated adenovirus serotype 5 vectors. Blood 116, 2656–2664.

Baker, A.H., Nicklin, S.A., and Shayakhmetov, D.M. (2013). FX and host defense evasion tactics by adenovirus. Mol. Ther. 21, 1109–1111.

Belin, M.T., and Boulanger, P. (1993). Involvement of cellular adhesion sequences in the attachment of adenovirus to the HeLa cell surface. J. Gen. Virol. 74 (Pt 8), 1485–1497.

Bergelson, J.M., Cunningham, J.A., Droguett, G., *et al.* (1997). Isolation of a common receptor for Coxsackie B viruses and adenoviruses 2 and 5. Science 275, 1320–1323.

Boulanger, P.A., and Puvion, F. (1973). Large-scale preparation of soluble adenovirus hexon, penton and fiber antigens in highly purified form. Eur. J. Biochem. 39, 37–42.

Bradshaw, A.C., Coughlan, L., Miller, A.M., *et al.* (2012). Biodistribution and inflammatory profiles of novel penton and hexon double-mutant serotype 5 adenoviruses. J. Control. Release 164, 394–402.

Chen, C.Y., May, S.M., and Barry, M.A. (2010). Targeting adenoviruses with factor x-single-chain antibody fusion proteins. Hum. Gene Ther. 21, 739–749.

Conway, J.F., and Steven, A.C. (1999). Methods for reconstructing density maps of ''single'' particles from cryoelectron micrographs to subnanometer resolution. J. Struct. Biol. 128, 106–118.

Corjon, S., Gonzalez, G., Henning, P., *et al.* (2011). Cell entry and trafficking of human adenovirus bound to blood factor X is determined by the fiber serotype and not hexon:heparan sulfate interaction. PLoS One 6, e18205.

Coughlan, L., Alba, R., Parker, A.L., *et al.* (2010). Tropism-modification strategies for targeted gene delivery using adenoviral vectors. Viruses 2, 2290–2355.

Doronin, K., Flatt, J.W., Di Paolo, N.C., *et al.* (2012). Coagulation factor X activates innate immunity to human species C adenovirus. Science 338, 795–798.

Duffy, M.R., Parker, A.L., Kalkman, E.R., *et al.* (2013). Identification of novel small molecule inhibitors of adenovirus gene transfer using a high throughput screening approach. J. Control. Release 170, 132–140.

Fabry, C.M., Rosa-Calatrava, M., Conway, J.F., *et al.* (2005). A quasi-atomic model of human adenovirus type 5 capsid. EMBO J. 24, 1645–1654.

Franqueville, L., Henning, P., Magnusson, M., *et al.* (2008). Protein crystals in adenovirus type 5-infected cells: requirements for intranuclear crystallogenesis, structural and functional analysis. PLoS One 3, e2894.

Fuller, S.D., Butcher, S.J., Cheng, R.H., and Baker, T.S. (1996). Three-dimensional reconstruction of icosahedral particles—the uncommon line. J. Struct. Biol. 116, 48–55.

Gout, E., Schoehn, G., Fenel, D., *et al.* (2010). The adenovirus type 3 dodecahedron's RGD loop comprises an HSPG binding site that influences integrin binding. J. Biomed. Biotechnol. 2010, 541939.

Irons, E.E., Flatt, J.W., Doronin, K., *et al.* (2013). Coagulation factor binding orientation and dimerization may influence infectivity of adenovirus-coagulation factor complexes. J. Virol. 87, 9610–9619.

Khare, R., Reddy, V.S., Nemerow, G.R., and Barry, M.A. (2012). Identification of adenovirus serotype 5 hexon regions that interact with scavenger receptors. J. Virol. 86, 2293–2301.

Marttila, M., Persson, D., Gustafsson, D., *et al.* (2005). CD46 is a cellular receptor for all species B adenoviruses except types 3 and 7. J. Virol. 79, 14429–14436.

Mittal, S.K., Mcdermott, M.R., Johnson, D.C., *et al.* (1993). Monitoring foreign gene expression by a human adenovirus-based vector using the firefly luciferase gene as a reporter. Virus Res. 28, 67–90.

Molinier-Frenkel, V., Gahery-Segard, H., Mehtali, M., *et al.* (2000). Immune response to recombinant adenovirus in humans: capsid components from viral input are targets for vector-specific cytotoxic T lymphocytes. J. Virol. 74, 7678–7682.

Molinier-Frenkel, V., Lengagne, R., Gaden, F., *et al.* (2002). Adenovirus hexon protein is a potent adjuvant for activation of a cellular immune response. J. Virol. 76, 127–135.

Nilsson, E.C., Storm, R.J., Bauer, J., *et al.* (2011). The GD1a glycan is a cellular receptor for adenoviruses causing epidemic keratoconjunctivitis. Nat. Med. 17, 105–109.

Russell, W.C. (2009). Adenoviruses: update on structure and function. J. Gen. Virol. 90, 1–20.

Sirena, D., Lilienfeld, B., Eisenhut, M., *et al.* (2004). The human membrane cofactor CD46 is a receptor for species B adenovirus serotype 3. J. Virol. 78, 4454–4462.

Sunnerhagen, M., Forsen, S., Hoffren, A.M., *et al.* (1995). Structure of the Ca(2+)-free Gla domain sheds light on membrane binding of blood coagulation proteins. Nat. Struct. Biol. 2, 504–509.

Vigant, F., Descamps, D., Jullienne, B., *et al.* (2008). Substitution of hexon hypervariable region 5 of adenovirus serotype 5 abrogates blood factor binding and limits gene transfer to liver. Mol. Ther. 16, 1474–1480.

Waddington, S.N., Mcvey, J.H., Bhella, D., *et al.* (2008). Adenovirus serotype 5 hexon mediates liver gene transfer. Cell 132, 397–409.

Wang, H., Li, Z.Y., Liu, Y., *et al.* (2011). Desmoglein 2 is a receptor for adenovirus serotypes 3, 7, 11 and 14. Nat. Med. 17, 96–104.

Wickham, T.J., Mathias, P., Cheresh, D.A., and Nemerow, G.R. (1993). Integrins alpha v beta 3 and alpha v beta 5 promote adenovirus internalization but not virus attachment. Cell 73, 309–319.

Xu, Z., Qiu, Q., Tian, J., *et al.* (2013). Coagulation factor X shields adenovirus type 5 from attack by natural antibodies and complement. Nat. Med. 19, 452–457.

Address correspondence to:
Dr. Pascal Fender
Unit of Virus Host Cell Interactions (UMI-3265)
6 rue Jules Horowitz
38042 Grenoble
France

E-mail: pfender@embl.fr

Received for publication December 11, 2013;
accepted after revision February 5, 2014.

Published online: February 10, 2014.